Final Draft
of the original manuscript:

Balejcikova, L.; Haramus, V.M.; Avdeev, M.V.; Petrenko, V.I.; Almasy, L.; Kopcansky, P.:

The effect of solution pH on the structural stability of magnetoferritin

In: Colloids and Surfaces B (2017) Elsevier

DOI: 10.1016/j.colsurfb.2017.05.036

The effect of solution pH on the structural stability of magnetoferritin

L. Balejčíková[1], V. M. Garamus[2], M. V. Avdeev[3], V. I. Petrenko[3,4], L. Almásy[5,6], P. Kopčanský[1]

[1]Institute of Experimental Physics, Slovak Academy of Sciences, Watsonova 47 04001 Košice, Slovakia

[2]Helmholtz-Zentrum Geesthacht: Centre for Materials and Coastal Research, Max-Planck-Street 1, 21502 Geesthacht, Germany

[3]Joint Institute for Nuclear Research, Joliot-Curie 6, 141980 Dubna, Moscow Region, Russia

[4]Kyiv Taras Shevchenko National University, Volodymyrska Street 64, Kyiv 01033, Ukraine

[5]State Key Laboratory Cultivation Base for Nonmetal Composites and Functional Materials, Southwest University of Science and Technology, Mianyang 621010, China

[6]Wigner Research Centre for Physics, Hungarian Academy of Sciences, H-1525, Budapest POB 49, Hungary

Abstract

The structural stability of magnetoferritin, a synthetic analogue of ferritin, at various pH levels is assessed here. The structural and electrical properties of the complexes were determined by small-angle X-ray scattering (SAXS), dynamic light scattering (DLS) and zeta potential measurements. At pH 3–6 a reduction of electrostatic repulsion on the suspended colloids resulted in aggregation and sedimentation of magnetoferritin. At neutral to slightly alkaline conditions (pH 7–9) the magnetoferritin structure was stable for lower iron loadings. Higher solution pH 10 – 12 induced destabilization of the protein structure and dissociation of subunits. Increasing the loading factor in the MFer complex leads to decrease of the stability versus pH changes.

Keywords: structure and stability, magnetoferritin solution, pH-dependent structure, small-angle X-ray scattering, dynamic light scattering

1. Introduction

The development of a targeted drug delivery system that is uniform, biocompatible, biodegradable, stable and non-toxic remains an exacting challenge because the therapeutic effects of the drug may be reduced by the partial degradation of the carrier before it has reached the target. To achieve the stated goal researchers are turning to nanoarchitectonics to design robust, ordered 3D membranous structures that contain nanochannels for enhanced therapeutic

drug delivery. For investigations of these complex systems high resolution imaging and scattering methods provide a valuable support [1].

An attractive system for drug binding is the iron storage protein – ferritin because it has an empty nano-size spherical protein shell 12 nm in outer radius and 8 nm in internal radius, i.e., an internal cavity where drug molecules can be encapsulated [2]. The protein surfaces of apoferritin also contain numerous binding sites for coupling with various antibodies, small molecules, peptides, signal molecules, drugs or dyes [36]. The superparamagnetic analogue of apoferritin, magnetoferritin (MFer) is also a potential magneto-pharmaceutical nanomaterial. MFer is usually characterized, similarly as ferritin, as a complex but with magnetic nanoparticles encapsulated within the native protein (apoferritin) by controlled *in vitro* Fe^{3+} loading. This type of complex could be used for targeted drug delivery using external magnetic field or for magnetic hyperthermia therapy [7,8].

The physico-chemical properties of MFer are well-known. From the first synthesis in 1992 [9] by a broad range of experimental techniques, such as SQUID magnetometry [10-13], Mössbauer spectroscopy [14-16], transmission electron microscopy [9,11,16,17], atomic force microscopy [16], electron magnetic resonance [17], magneto-optical methods [18,19], dynamic light scattering (DLS), small-angle neutron (SANS) and X-ray (SAXS) scattering [20,21]. Detailed research of MFer is important due to the high potential of its applications especially in the biomedical field of science, e.g. as contrast agent in radiology, a drug carrier in the targeted transport, or a standard in diagnostics of various diseases) [7,22]. Similarly to ferritin, MFer can bind to damaged human cells by protein interactions with overexpressed transferrin receptor (TfR1) highly expressed on human cancer cells and could be used as a targeting marker for tumor diagnosis by MRI and targeted therapy [22,23]. Moreover, the presence of the magnetic nanoparticles in MFer results in a dramatic increase in the sensitivity of MRI to the T_2 relaxation [24]. Previous SAXS studies have shown that the MFer protein shell structure is influenced by the loading factor (LF – the average number of Fe atoms per macromolecule). Structural changes were observed at LF above ~150, such as partial destruction of MFer [20]. It was concluded [20,21], that the structural and size polydispersity was affected by the presence of iron, and the high iron oxide : protein ratio caused the damage of the shell. However, in these studies certain physico-chemical conditions, such as the pH, have not been controlled and it was not clarified, how pH changes related to forming complexes with drugs would affect the behavior of MFer. The variation of MFer structure at different pH could induce modifications of the protein surface and drug binding depending on specific properties of the substance or the binding mechanism.

The importance and role of pH on the structure of the parent molecule, apoferritin, is well documented [25-28]. Apoferritin is comprised of 24 subunits joined by non-covalent bonds. Through interaction of protein subunits, the assembled quaternary structure of the functional protein is formed, capable of catalyzing the uptake and release of iron according to specific requirements of organism [29-30]. The *in vitro* self-assembly mechanism of apoferritin isolated from horse spleen after reversible dissociation of protein subunits under the influence of pH change was first proposed by Gerl et al. [25,26] based on of intrinsic fluorescence, far-UV circular dichroism and glutaraldehyde cross-linking experiments. The pH-dependent SAXS study by Kim and co-authors [27] has brought a new insight into the formation mechanism of apoferritin. In that work, destruction of apoferritin shell was observed below the critical pH = 3.40. Apoferritin disassembly and reassembly was shown to be not fully reversible by changing pH, and the ferrihydrite core of ferritin aggregated below pH 2.10 [27]. The latest SAXS and DLS study of apoferritin in the pH range 2 - 7.4 has shown similar results [28]. Based on the mentioned previous investigations, in a number works it was shown successful construction of the (apo)ferritin complex with anticancer drugs (e.g. doxorubicin, cisplatin, carboplatin, oxaliplatin, methylene blue or daunomycin) achieved through manipulating the pH-dependent unfolding-refolding process of (apo)ferritin in saturated drug solutions [23, 31-35]. Moreover, pH-dependent iron release from ferritin-containing core was recently reported [36-38]. Similar investigations of the pH related properties of MFer are necessary for further biomedical applications of MFer system.

Solution pH is closely related to the structure, stability, activity and function of proteins. Talley and E. Alexov [39] found that the pH-optimum of proteins activity correlates with stability Therefore, we consider that the discovered peroxidase-like activity of MFer observed at pH 7.04 [40] and destructive activity of MFer on lysozyme amyloid fibrils (pH ~ 6) related to magnetic nanoparticles presence [41] could be also affected by pH changes.

The purpose of our work is to (1) establish the structural properties as a function of the solution pH; (2) find the optimal range in which MFer is stable and not aggregated; and (3) find the optimal range in which MFer forms a homogenous dispersion for future binding with various substances followed by bio-applications. Preliminary studies of colloidal stability suggest that the isoelectric point (pI), the point of the lowest stability at defined pH value (at which protein precipitation occur and the total charge of protein is zero) determined for magnetoferritin with loading factor 1250, was 4.52 ± 0.05 [42] in comparison with pure apoferritin (4.58 ± 0.02) [43]. However, the parameter pI, which depends on the chemical properties of the solvent, gives no information on the possible protein structural changes. Other

methods, such as magnetometry or Mössbauer spectroscopy cannot give proper information on the size and composition of the MFer complex and variability of its structure. In our previous study [44] we used SQUID magnetometry to characterize the magnetic properties of magnetoferritin samples with various loading factors. We found that the width (FWHM) of the blocking temperature peak decreased with an increase in the loading factor, an indication that particle size distribution became narrower as the concentration of iron in the biomacromolecule increased. Transmission electron microscopy or atomic force microscopy provides direct structural information, with disadvantages of low statistics and inability of assessing the intrinsic properties. Highly efficient structure-sensitive methods that provide a statistically averaged picture of the whole sample are scattering methods. In particular the popularity of SAXS continues to grow with the development of new powerful sources of radiation and data analysis methods. In this study we probe the structure of MFer, by using the SAXS method as a function of MFer iron loading and solution pH.

2. Materials and methods

Materials

Ammonium ferrous sulfate hexahydrate ($(NH_4)_2Fe(SO_4)2.6H_2O$), Equine Spleen Apoferritin in 0.15 M NaCl, hydrogen peroxide (H_2O_2), potassium thiocyanate (KSCN), sodium hydroxide (NaOH), trimethylamine N-oxide (Me_3NO) and 3-[(1,1-dimethyl-2-hydroxyethyl)amino]-2-hydroxypropanesulfonic acid (AMPSO) were purchased from Sigma-Aldrich, Coomassie brilliant blue from Fluka, hydrochlorid acid (HCl) from ITES, potassium thiocyanate (KSCN) from Slavus, ethanol (C_2H_6O) and phosphoric acid (H_3PO_4) from Centralchem, demineralized water.

Sample preparation

All samples were prepared at the Department of Magnetism of the Institute of Experimental Physics of the Slovak Academy of Sciences in Kosice, Slovakia, and were subjected to basic physico-chemical characterizations. Magnetoferritin was synthetized by procedure described previously [44]. After synthesis, exact pH values were adjusted using various amounts of 0.2 M HCl and 2 M NaOH and pH was measured using Mettler Toledo SevenEasy S20-KS pH meter and Mettler Toledo Inlab®SciencePro pH electrode. For comparison purpose, apoferritin solutions were prepared by dissolution of commercial

apoferritin in AMPSO buffer and various pH were achieved by the same process as that for MFer case.

Measurement of loading factor

Loading factor (the average number of iron atoms per one apoferritin biomacromolecule) has been determined using UV-VIS spectrophotometry SPECORD 40 Analytik Jena at the temperature 25°C with precision about 1% by methods described previously [44].

Determination of hydrodynamic diameter (<D_{HYDR}>) *by dynamic light scattering (DLS)*

Dynamic light scattering, also known as photon correlation spectroscopy or quasi-elastic light scattering measurements, were recorded on a Zetasizer Nano ZS 3600 (Malvern Instruments) at 25°C [45]. A sample was suspended in 0.05 M AMPSO buffer using disposable polystyrene cuvettes, and experiments performed in triplicate with each measurement taking about one minute. An estimate of the standard error of a measurement is represented by the error bars on the <D_{HYDR}> vs pH plots. With the instrument in "protein mode" the average hydrodynamic diameter <D_{HYDR}> was obtained from the maximum of the particle size from number weighed distribution curve, displayed in Zetasizer software.

Zeta potential measurements

Zeta potential was measured using Laser Doppler velocimetry combined with electrophoresis on Zetasizer Nano ZS 3600 (Malvern Instruments) at 25°C.

The zeta potential, ζ, parameter of the colloidal stability, measured in mV, generates between the particle (protein) surface with its electric double layer and the dispersing liquid and varies according to the distance from the particle surface [45].

Zeta potential measurements were performed within one minute after filling of folded capillary cells, using monomodal mode of data analysis.

SAXS experiment

SAXS measurements were recorded at the P12 BioSAXS beam-line of the European Molecular Biology Laboratory (EMBL) at the storage ring PETRA III of the Deutsche Elektronen Synchrotron (DESY, Hamburg, Germany) at 20°C using a Pilatus 2M detector (1475 × 1679 pixels) (Dectris, Switzerland) and synchrotron radiation with a wavelength 0.1 nm. The sample-detector distance was 3 m, allowing for measurements in a *q*-range of 0.03-4.4

nm^{-1}. The *q*-range was calibrated using the diffraction patterns of silver behenate. The experimental data were normalized to the transmitted beam intensity, corrected for a non-homogeneous detector response, and the background scattering of the aqueous buffer was subtracted. An automatic sample changer for a sample volume of 20 μL was used. The experimental time including sample loading, exposure, cleaning and drying was about 1 min per sample. The solvent scattering was measured before and after the sample scattering in order to control the eventual sample holder contamination. Twenty diffraction patterns were collected for every sample, each with an exposure time of 0.05 s. To avoid radiation damage by subsequent illuminations, curves showing deviations were discarded. The final scattering curve was obtained using the automated acquisition and analysis by averaging the scattering data collected from different frames [46, 47].

Some samples, in which sedimentation was observed, were measured immediately after mixing and after 10 minutes centrifugation at the supernatant phase.

The scattering curves were modelled by monodisperse approximation for spherical shell, analyzed by indirect Fourier transformation, using and GNOM [48] programs from reciprocal to real space for construction of pair distance distribution functions *p(r)* (the distribution of distances between all pairs of points within the particle weighted by the respective electron densities [49]). *Ab initio* models were constructed by DAMMIF [50] and visualized using Raswin program.

3. Results

3.1 Average size and stability vs pH (DLS)

In order to study pH effects, different magnetoferritin samples with loading factors 97, 295, 310, 421 and 511 were prepared. The average hydrodynamic diameter, $<D_{HYDR}>$, of MFer and apoferritin in aqueous solution was obtained by dynamic light scattering (DLS). For low LF, the behaviour is similar to apoferritin and differences are visible for higher LF. The measured hydrodynamic diameter ($<D_{HYDR}>$) varied as a function of pH (Fig. 1a), while at low pH values 2 – 6 for MFer with LF 97 – 511 $<D_{HYDR}>$ increased above 10 μm which was over the detection limit. The general behavior is, that $<D_{HYDR}>$ of MFer samples increases with LF growth.

3.2 Electrical charge vs pH (zeta potential)

Data in Fig. 1b indicates that the lowest colloidal stability of samples is around pH 4. Isoelectric point of samples was 4.6 ± 0.02 for apoferritin, 4.6 ± 0.03 for MFer LF 97, 4.6 ±

0.05 for MFer LF 295, 4.7 ± 0.04 for MFer LF 310, 4.6 ± 0.05 for MFer LF 421 and 4.4 ± 0.07 for MFer LF 511 (Fig. 1b). Zeta potential is related to the charge generated on the protein surface. Negative zeta potential is the negative total charge of the studied particle and positive zeta potential, the positive total charge [45]. Apof and MFer biomacromolecules in aqueous solution show negative zeta potential and negative total surface charge in AMPSO buffer medium without pH adjustment (Fig. 1b). If we added alkali to these solutions, particles will tend to acquire a negative charge. If acid was then added, the negative charge was neutralized, and further addition of acid caused building up of positive charge. All MFer and Apof samples at neutral and alkali pH values formed relatively stable colloidal dispersions.

3.3 Internal structure vs pH at different LF by SAXS

First, SAXS measurements of apoferritin and MFer with LF 97-511 were recorded at various pH values. Typical patterns are presented in Fig. 2a, 2b and 2c. Oscillation peaks at $q > 0.6$ nm^{-1}, characteristic for spherical shell, are visible only for Apof (Fig. 2a) and MFer with LF 97 (Fig. 2b). For magnetoferritin, minima and maxima are less pronounced, indicating that the spherical form of the protein is only partly preserved. The result is interpreted in terms of deformation of the protein shell upon iron loading, leading to a decrease in the spherical symmetry of the molecules. The increase in the scattering intensity at small values of q shows, that a fraction of the complexes undergo aggregation. Polydisperse vesicles formed by lipid molecules were previously observed and analyzed by Angelov et al. [51] using the SAXS technique. Comparing scattering curves for different pH values, the oscillations disappear at pH about 11, most likely a result of the dissociation of protein subunits. Due to the instability of MFer sample at pH 4.74 with LF 97 the scattering curve is not displayed in Fig. 2b. A maximum and minimum was not observed for scattering curves with LF 421 (Fig. 2c) in addition to any significant differences versus pH in this q region characteristic for the molecular shape. That is, the shape of apoferritin shell is affected by iron loading more strongly than by solution pH. Such high iron loading leads to destruction of the shell structure, as reported previously [20,21].

The $p(r)$ functions constructed for $q > 0.2$ nm^{-1} are shown in Fig. 2d for Apof, MFer with LF 97 and MFer with LF 421. The position of the maximum for Apof and MFer with LF 97 moves to smaller distance at higher pH due to dissociation of the shell. Similarly, aggregation of the protein shell and visible sedimentation at pH 2-6 within a few minutes correlated well with a larger distance. Specifically, sedimentation was observed for Apof at pH 4.84, MFer with LF 97 at pH 5.85, 4.74 and 3.70, MFer LF 295 at pH 5.60, 4.33 and 3.52, MFer

LF 310 at pH 4.90, 3.31 and 2.33, MFer LF 421 at pH 5.91, 4.66 and 3.65 and MFer LF 511 at pH 4.97, 3.37 and 2.47. The effect is graphically illustrated by Fig. 3a for MFer with LF 97 at various pH values. For visualization of the structure for different pH values, *ab initio* models for Apof and MFer with LF 97 are presented in Fig. 4.

Samples that were not stable between pH 2 and pH 6 were measured as supernatants after separation of aggregates by centrifugation for 10 minutes at 10 000 rpm to confirm the presence or absence of protein biomacromolecules in solution. For illustration we compared Apof at pH 4.84 with supernatant and Apof at stable pH 8.36, Fig. 5. Apof at pH 8.36 without aggregation was well-described by a simple core-shell model. We observed the presence of apoferritin shells also in the supernatant of colloidal system with MFer with LF 97 at pH 5.85 and MFer with LF 421 at pH 5.91. MFer in this acidic pH condition is characterized by the enormous polymorphism and the coexistence of large protein based fractal-like structures with the core-shell apoferritin biomacromolecules not influenced by H^+ ions or iron ions binding. Similar SANS curves (scattering from pure apoferritin shell) were observed for supernatant solution from quite high LF=910 [21]. These observations are most likely associated with an increase in iron loading, and this turn related to the lowering of the solution pH. Nevertheless the pH level after the synthesis was not below neutral, an indication that the precipitation was due to a specific effect of iron oxide formation inside magnetoferritin that was also responsible for the destruction of the protein shell [20, 21]. From the structural study we conclude that

(i) low pH has similar effect on structure and stability of MFer complexes as the increase of LF; and

(ii) the difference between low pH and high iron loading effects on the stability of magnetoferritin is related to H^+ binding and iron oxide respectively.

4. Discussion

Dynamic light scattering measurements for apoferritin and MFer with LF 97-511 (Fig. 1a) are in qualitative agreement with our previous results [20]. Dynamic light scattering and SAXS measurements show the same trend of average size of aggregates. As DLS detects the particles plus hydration shell and SAXS sees the ”dry particles”, one can conclude that the presence of the hydration shell had no effect on the observation of the aggregation behavior.

On the other hand, the hydrodynamic diameter of MFer with LF 421 and 511 increased strongly due to the presence of higher iron loading. Thus, the peak in hydrodynamic diameter versus pH for the biggest LF 511 can be interpreted in terms of protein-protein interactions.

The behavior of zeta potential versus pH for apoferritin and magnetoferritin at various loading factors was rather similar (Fig. 1b) because of the similar charge distribution on the protein surface. On the other hand, the structure of MFer depends very strongly on pH and LF because of the presence of iron and H^+ removal or binding from the protein surface, which could affect the protein structure. As noted in the Introduction, at the isoelectric point the positive and negative charges on the protein are balanced, and the protein has zero net charge. Accordingly, the isoelectric point was used to define zero zeta potential at which the protein exhibited the lowest stability and flocculated. Fig. 1 b (insert) illustrates the dependence of the isoelectric point on the loading factor.

In general, SAXS data for pure Apof agree with results reported by Kim et al. [27]. At pH 4.84 we observe a slope at low *q*, typical for particle agglomeration, whereas Kim et al. reported aggregation only below pH 1.0, attributed to pH-induced denaturation of apoferritin. In a recent study Ciasca et al. [28] have shown, that apoferritin subunits are gradually released in solution between critical pH 3.5 and 2. These differences can be caused by various factors, discussed below. The Apof samples in [27] may have been measured after separation (sedimentation, filtration or centrifugation) of the large aggregates. Another explanation can be related to the reaction kinetics after addition of HCl. Samples measured immediately after pH change may not show any aggregation since the process is often time dependent. As the study of reaction kinetics was not the main goal of our work, our samples were measured after ~ 48 hours of their preparation. Meanwhile, our samples could be exposed to the time-dependent "digestion" after addition of HCl. These hypotheses cannot be confirmed as the precise reaction time or use of separation method was not mentioned in Kim's study. Another important point to be considered is the medium: in Kim´s work it was 0.15 M NaCl solution, and in our work 0.05 M AMPSO buffer solution; such difference could also influence the stability of samples. Protein concentration was also different. In contrast with Kim, who used a broad concentration range 1 – 10 mg/mL, we have used a narrower concentration range between 3.6 – 7.1 mg/mL (see description below Fig. 2a, 2b and 2c). For one LF, the concentration was changed due to the additions of 0.2 M HCl and 2 M NaOH solutions. In general, higher protein concentrations could affect interactions between particles, promoting their aggregation.

Magnetoferritin with the lowest loading factor 97 showed the presence of large agglomerates, an indication of the effect of iron binding. Therefore, to achieve a high iron loading and colloidal stability, the concentration of protein must be lower than that used in our previous work, 0.7 mg/mL [44]. Alternatively, to maintain stability and avoid agglomeration the post-synthesis pH level must be increased from neutral to 8-9. This pH adjustment would

not only induce repulsive interactions between protein macromolecules but also break-up the large agglomerates.

Structures visualized by *ab initio* modeling for Apof and MFer at the lowest LF 97 were compared. Dissociation of Apof structure to subunits at pH 11.31 (Fig. 4) by removal of H^+ ions from side chain groups on the protein surface leads to formation of rod-like oligomers; with decreasing pH the core–shell structure becomes more folded. Between pH 6 – 8 the structure seems to be compact, a result we attributed to electrostatic repulsion forces between the negatively charged biomacromolecules (see Fig. 1b). This perforated, atypical structure may be associated with chemical conditions and ionic strength of the 0.05 M AMPSO buffer solution or result from exposure to acidic pH conditions could cause "digestion" of the shell. Fundamental structural biology suggests that small pH changes around pH optimum can result in binding or removal of H^+ ions from side chain groups on the surface of a protein without causing any permanent damage to the protein conformation. Rapid pH changes, mainly in acidic conditions, can affect salt bridges and hydrogen bonding and change the attractions between the groups in the side chains of the amino acids that determine the final shape of a protein and cause pH-induced protein denaturation. It should be noted that all *ab initio* pictures represent an average structure, while the solution may also contain complete shells, as we observed in Apof supernatant (Fig. 5). *Ab initio* models for MFer with LF 97 point to the destroyed or partially unfolded shell for all pH values (Fig. 4).

Finally, we have measured unstable samples after phase separation as supernatant liquid. In all cases (Apof, MFer with LF 97 and 421) the supernatant liquids contained monodisperse structures which were described well as core-shell particles. That is, some part of Apof biomacromolecules was not affected by the interaction with H^+ ions in acidic pH (Fig. 5). This observation can indirectly confirm our suggestion that Kim might have worked with separated Apof samples as supernatants. Typical minima and maxima are visible at pH 4.20 in Kim's data and in our data for supernatants. MFer supernatant significantly differs from MFer at the same stable pH values, that may be interpreted in terms of a part of the biomacromolecule does not bind H^+ and / or is unable to bind any iron to form MFer complex. This observation suggests that MFer solutions contained core-shell structures as well as destroyed unstable structures that flocculated and could not be studied in detail.

5. Summary

We presented results on the influence of pH on the structure of magnetoferritin and apoferritin, using a combination of dynamic light scattering, zeta potential and small-angle X-

ray scattering. DLS data have shown the change of hydrodynamic diameter with pH that could be caused by conformation changes of protein or (dis)assembling protein mechanisms due to the H^+ release or binding. Zeta potential measurements have shown that magnetoferritin surface is negatively charged at pH 5 – 12 and positively at pH 2 – 4. SAXS data indicated the region of the lowest stability of magnetoferritin at pH 3 – 6, as shown by the presence of larger aggregates. Magnetoferritin samples were the most stable between pH 7 – 9, the optimum pH range for bio-applications. Protein dissociation started at pH ~ 10 and was pronounced at pH ~ 12. The stability versus pH decreased with higher iron loading.

Acknowledgements

This work was supported by the project of the Slovak Scientific Grant Agency VEGA (project No. 2/0016/17), the Slovak Research and Development Agency under the contract No. APVV-015-0453 and by the Ministry of Education Agency for European Structural funds (projects No. 26220120033, No. 26210120012 and No. 26220220186). We thank Mark J. Henderson for his careful and critical reading of the manuscript. The support of Clement Blanchet (EMBL) is kindly acknowledged.

References:

[1] A. Angelova, B. Angelov, R. Mutafchieva, S. Lesieur, J Inorg Organomet Polym 25 (2015) 214.

[2] E. C. Theil, R. K. Behera, T. Tosha, Coord. Chem. Rev. 257 (2013) 579-586.

[3] J. F. Hainfeld, Proc. Natl. Acad. Sci. U S A 89 (1992) 11064.

[4] F. Liu, B. Du, Z. Chai, G. Zhao, F. Ren, X. Leng, Eur. Food Res. Technol. 235 (2012) 893.

[5] Z. Zhen, W. Tang, H. Chen, X. Lin, T. Todd, G. Wang, T. Cowger, X. Chen, J. Xie, ACS Nano 7 (2013) 4830.

[6] P. Huang, P. Rong, A. Jin, X. Yan, M. G. Zhang, J. Lin, H. Hu, Z. Wang, X. Yue, W. Li, G. Niu, W. Zeng, W. Wang, K. Zhou, X. Chen, Adv. Mater. 26 (2014) 6401.

[7] E. C. Theil, R. K. Behera, T. Tosha, Coord. Chem. Rev. 257 (2013) 579.

[8] Babincová M, Leszczynska D, Sourivong P and Babinec P Med. Hypotheses 54 (2000) 177

[9] F. C. Meldrum, B. R. Heywood, S. Mann, Science 257 (1992) 522.

[10] J. W. Bulte, T. Douglas, S. Mann, R. B. Frankel, B. M. Moskowitz, R. A. Brooks, C. D. Baumgarner, J. Vymazal, J. A. Frank, Invest. Radiol. 29 (1994) 214.

[11] K. K. W. Wong, T. Douglas, S. Gider, D. D. Awschalom, S. Mann, Chem. Mater. 10 (1998) 279.

[12] O. Kasyutich, A. Sarua, W. Schwarzacher, J. Phys. D: Appl. Phys. 41 (2008) 134022.

[13] O. Kasyutich, D. Tatchev, A. Hoell, F. Ogrin, C. Dewhurst, W. Schwarzacher, J. Appl.Phys. 105 (2009) 07B528.

[14] D. P. E. Dickson, S. A. Walton, S. Mann, K. Wong, NanoStruct. Mater. 9 (1997) 595.

[15] Q. A. Pankhurst, S. Betteridge, D. P. E. Dickson, T. Douglas, S. Mann, R. B. Frankel, Hyperfine Interact. 91 (1994) 847.

[16] M. J. Martinez-Perez, R. de Miguel, C. Carbonera, M. Martínez-Júlvez, A. Lostao, C. Piquer, C. Gómez-Moreno, J. Bartolomé, F. Luis, Nanotechnology 21 (2010) 465707.

[17] F. Moro, R. de Miguel, M. Jenkins, C. Gómez-Moreno, D. Sells, F. Tuna, E. J. L. McInnes, A. Lostao, F. Luis, J. van Slageren, J. Magn. Magn. Mater. 361 (2014) 188.

[18] M. Koralewski, M. Pochylski, Z. Mitróová, M. Timko, P. Kopčanský, L. Melníková. J. Magn. Magn. Mater. 323 (2011) 2413.

[19] M. Koralewski, J. W. Kłos, M. Baranowski, Z. Mitroova, P. Kopcansky, L. Melnikova, M. Okuda, W. Schwarzacher, Nanotechnology 23 (2012) 355704.

[20] L. Melnikova, V. I. Petrenko, M. V. Avdeev, V. M. Garamus, L. Almásy, O. I. Ivankov, L. A. Bulavin, Z. Mitróová, P. Kopčanský, Coll. Surf. B, 123 (2014) 82.

[21] L. Melnikova, V. I. Petrenko, M. V. Avdeev, O. I. Ivankov, L. A. Bulavin, V. M. Garamus, L. Almásy, Z. Mitroova, P. Kopcansky, J. Magn. Magn. Mater. 377 (2015) 77.

[22] K. Fan, C. Cao, Y. Pan, D. Lu, D. Yang, J. Feng, L. Song, M. Liang, X. Yan, Nat. Nanotechnol. 7 (2012) 459.

[23] M. Liang, K. Fan, M. Zhou, D. Duan, J. Zheng, D. Yang, J. Feng, X. Yan, Proc. Natl. Acad. Sci. U. S. A. 111 (2014) 14900.

[24] J. Wang, Y. Huang, A. E. David, B. Chertok, L. Zhang, F. Yu, V. C. Yang, Curr. Pharm. Biotechnol. 13 (2012) 2403.

[25] M. Gerl, R. Jaenicke, Eur. Biophys. J. 15(1987) 103.

[26] M. Gerl, R. Jaenicke, J. M. A. Smith, P. M. Harrison, Biochemistry 27 (1988) 4089.

[27] M. Kim, Y. Rho, K. S. Jin, B. Ahn, S. Jung, H. Kim, M. Ree, Biomacromolecules 12 (2011) 1629.

[28] G. Ciasca, M. Papi, M. Chiarpotto, G. Campi, R. D. Santo, R. Giordano, G. Maulucci, V. Palmieri, M. D. Spirito, Sci. Lett. J. 4 (2015) 210.

[29] E. C. Theil, H. Takagi, G. W. Small, L. He, A. R. Tipton, D. Danger, Inorg. Chim. Acta, 297 (2000) 242.

[30] D. Finazzi, P. Arosio, Arch. Toxicol. 88 (2014) 1787.

[31] Z. Yang, X. Wang, H. Diao, J. Zhang, H. Li, H. Sun, Z. Guo, Chem. Commun. (Camb.) 33 (2007) 3453.

[32] F. Yan, Y. Zhang, H.K. Yuan, M. K. Gregas, T. Vo-Dinh, Chem. Commun. (Camb.) 38 (2008) 4579.

[33] R. M. Xing, X. Wang, C. Zhang, Y. Zhang, Q. Wang, Z. Yang, Z. Guo, J. Inorg. Biochem. 103 (2009) 1039.

[34] A. H. Ma-Ham, H. Wu, J. Wang, X. Kang, Y. Zhang, Y. Lin, J. Mater. Chem. 21 (2011) 8700.

[35] M.A. Kilic, E. Ozlu, S. Calis, J. Biomed. Nanotechnol. 8 (2012) 508.

[36] N. Gálvez, B. Fernández, P. Sánchez, R. Cuesta, M. Ceolín, M. Clemente-León, S. Trasobares, M. López-Haro, J. J. Calvino, O. Stéphan, J. M. Domínguez-Vera. J. Am. Chem. Soc. 130 (2008) 8062.

[37] G. Ciasca, M. Papi, M. Chiarpotto, M. Rodio, G. Campi, C. Rossi, P. De Sole, and A. Bianconi. Appl. Phys. Lett. 100, 073703 (2012)

[38] M. Chiarpotto, G. Ciasca, M. Vassalli, C. Rossi, G. Campi, A. Ricci, B. Bocca, A. Pino, A. Alimonti, P. De Sole, and M. Papi. Appl. Phys. Lett. 103, 083701 (2013)

[39] K. Talley, E. Alexov, Proteins 78 (2010) 2699.

[40] L. Melníková, K. Pospiskova, Z. Mitróová, P. Kopčanský, I. Šafařík, Microchim. Acta, 181 (2014) 295.

[41] P. Kopcansky, K. Siposova, L. Melnikova, Z. Bednarikova, M. Timko, Z. Mitroova, A. Antosova, V. M. Garamus, V. I. Petrenko, M. V. Avdeev, Z. Gazova, J. Magn. Magn. Mater. 377 (2015) 267.

[42] Z. Mitróová, L. Melníková, J. Kováč, I. Vávra, M. Timko, P. Kopčanský, Magnetoferritin. In NANOCON 2011: 3rd International Conference, 21. – 23. 9. 2011, Brno, Česká Republika. Conference proceedings. - Ostrava: TANGER Ltd., 2011, p. 582-587. ISBN 978-80-87294-27-7.

[43] S. T. Silk, E. Breslow, J. Biol. Chem. 251 (1976) 6963.

[44] Z. Mitróová, L. Melníková, J. Kováč, M. Timko, P. Kopčanský, Acta Phys. Pol. A, 121 (2012) 1318.

[45] Zetasizer Nano Series: user manual. United Kingdom: Malvern Instruments Ltd., 2007. 292 p.

[46] D. Franke, A. G. Kikhney, D. I. Svergun, Nucl. Instrum. Methods A 689 (2012) 52.

[47] P. V. Konarev, V. V. Volkov, A. V. Sokolova, M. H. J. Koch, D. I. Svergun, J. Appl. Cryst. 36 (2003) 1277.

[48] D. I. Svergun, J. Appl. Crystallogr. 25 (1992) 495.

[49] D. I. Svergun, M. H. J. Koch, Rep. Prog. Phys. 66 (2003) 1735.

[50] D. Franke, D. I. Svergun, J. Appl. Cryst. 42 (2009) 342.

[51] B. Angelov, A. Angelova, V. M. Garamus, M. Drechsler, R. Willumeit, R. Mutafchieva, P. Štěpánek, S. Lesieur, Langmuir 28 (2012) 16647.

a.)

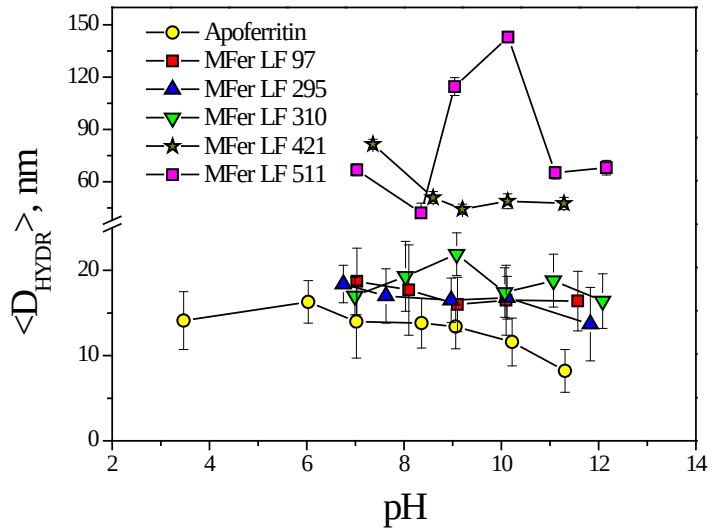

b.)

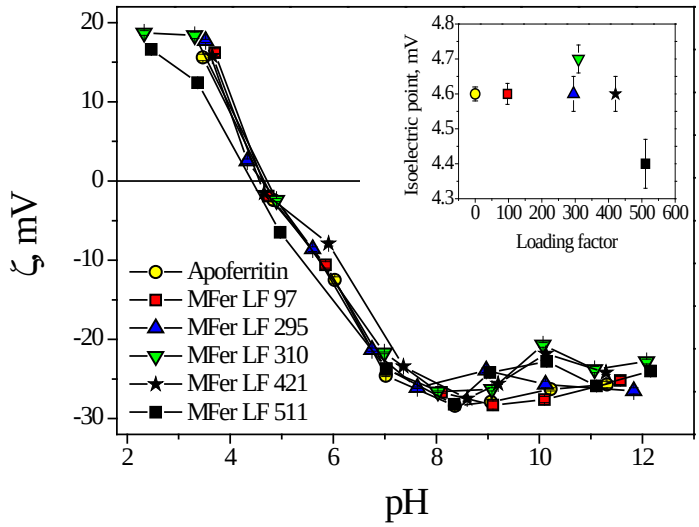

Fig. 1a. Comparison of hydrodynamic diameter $<D_{HYDR}>$ vs pH at different LF values and 1b. comparison of zeta potential vs pH at different LF values

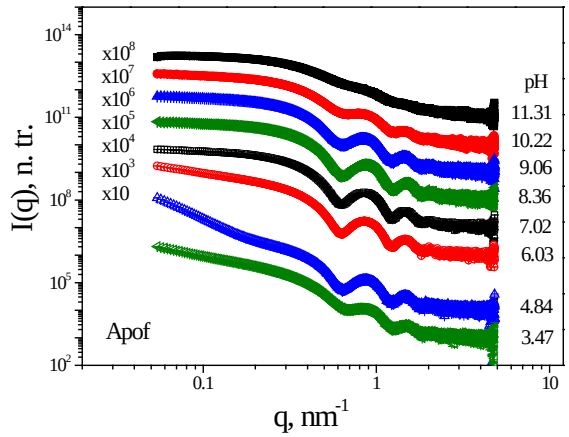

Fig. 2a. SAXS profiles of Apof measured at pH range 3.47-11.31 with protein concentration 7.1 mg/mL for pH 11.31, 7.1 mg/mL for pH 10.22, 7.2 mg/mL for pH 9.06, 7.3 mg/mL for pH 8.36, 7.0 mg/mL for pH 7.02, 7.0 mg/mL for pH 6.03, 6.9 mg/mL for pH 4.84 and 6.8 mg/mL for pH 3.47. Sedimentation was observed at pH 4.84.

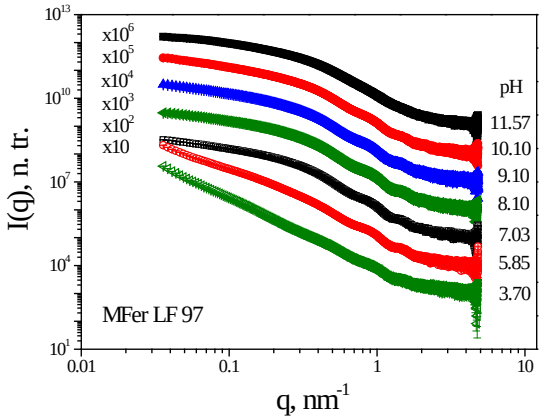

Fig. 2b. SAXS profiles of MFer with LF 97 measured at pH range 3.70-11.57 with protein concentration 5.6 mg/mL for pH 11.57, 5.6 mg/mL for pH 10.10, 5.7 mg/mL for pH 9.10, 5.8 mg/mL for pH 8.10, 5.6 mg/mL for pH 7.03, 5.6 mg/mL for pH 5.85 and 5.4 mg/mL for pH 3.70. Sedimentation was observed at pH 3.70, 4.74 and 5.85.

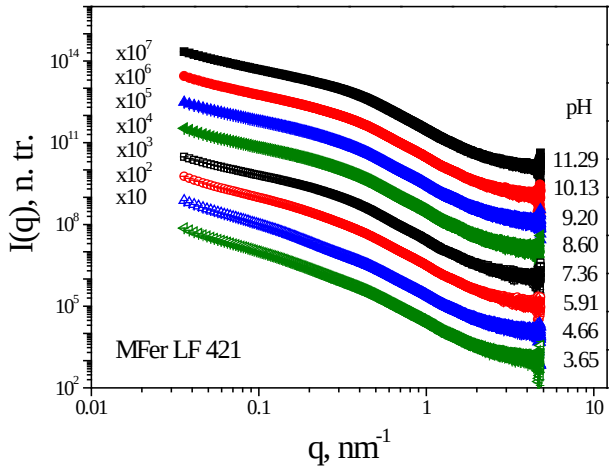

Fig. 2c. SAXS profiles of MFer with LF 421 measured at pH range 3.65-11.29 with protein concentration 5.6 mg/mL for pH 11.29, 5.7 mg/mL for pH 10.13, 5.8 mg/mL for pH 9.20, 5.8 mg/mL for pH 8.60, 5.5 mg/mL for pH 7.36, 5.4 mg/mL for pH 5.91, 5.3 mg/mL for pH 4.66 and 5.2 mg/mL for pH 3.65. Sedimentation was observed at pH 3.65, 4.66 and 5.91.

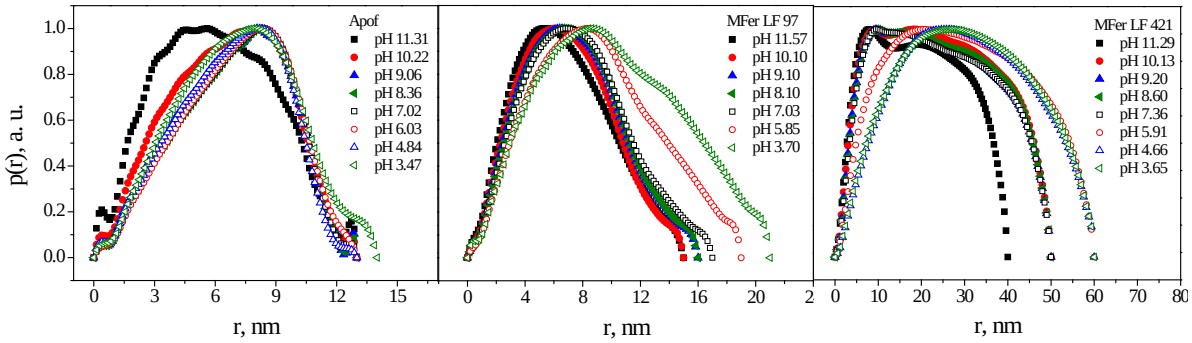

Fig. 2d. Pair distance distribution functions for Apof, MFer with LF 97 and MFer with LF 421 under various pH conditions, determined using GNOM program.

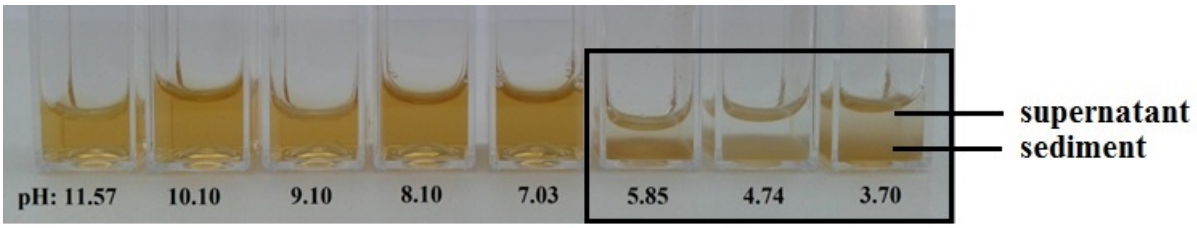

Fig. 3. Photographs of MFer sample with LF 97 with visible sedimentation at pH 5.85, 4.74 and 3.70.

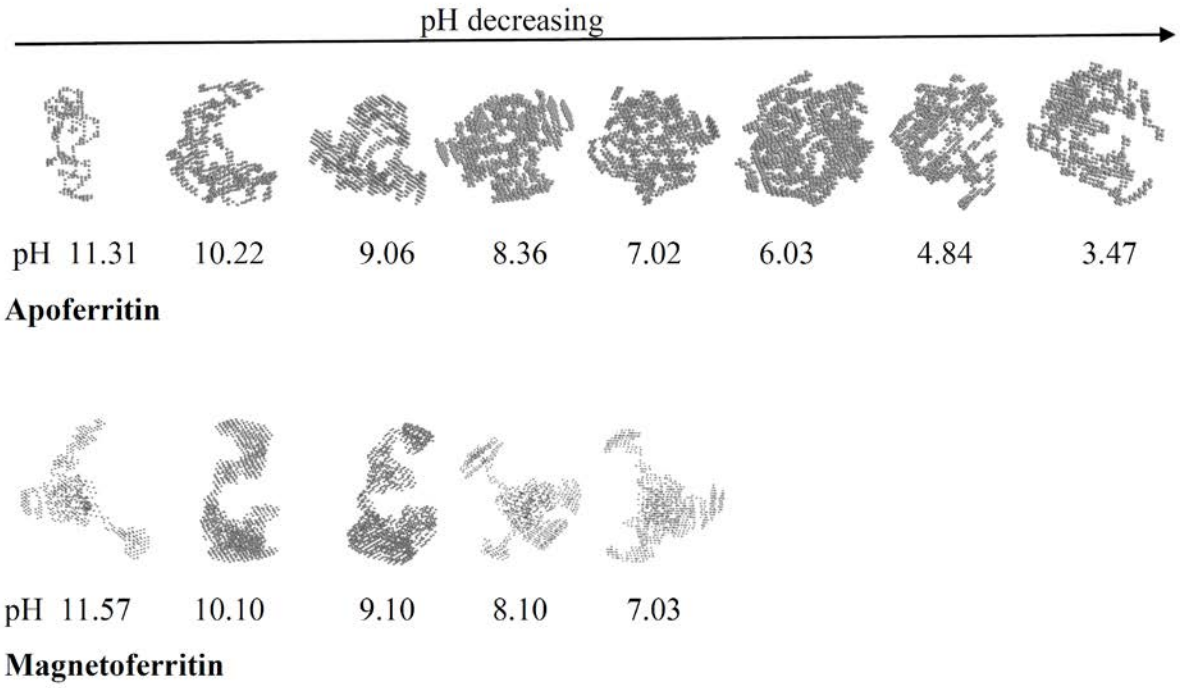

Fig. 4. *Ab initio* models of Apof and MFer with LF 97 at different pH values obtained by DAMMIF program.

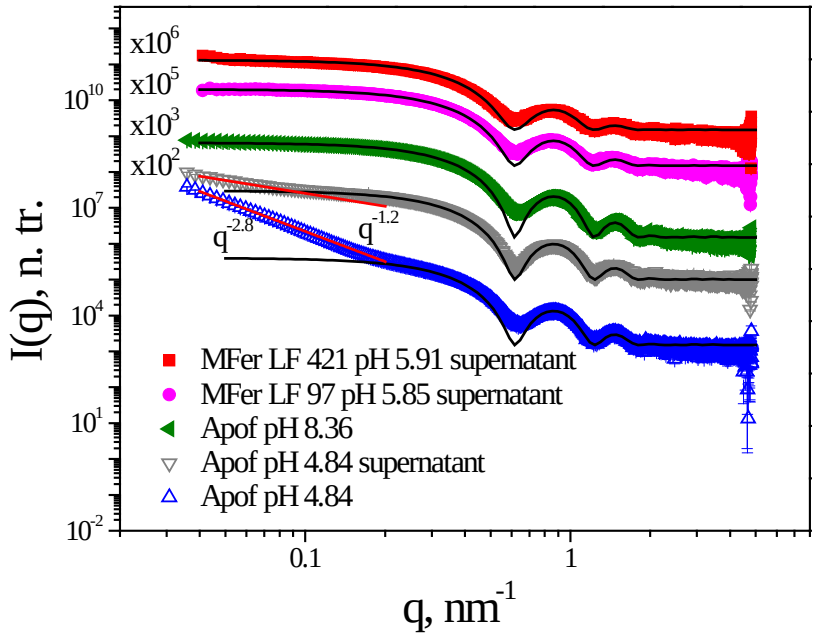

Fig. 5. Scattering curves of Apof at pH value 4.84 and supernatant are compared with stable pH 8.36. Supernatants of MFer LF 97 at pH 5.85 and MFer LF 421 at pH 5.91 are illustrated for comparison with Apof. SAXS data were analyzed by core-shell model with R_{OUTER} = 6.3 nm and R_{INNER} = 3.6 nm (black lines). The power law fits (red lines), applied for scattering curves of unstable Apof at q < 0.2 nm^{-1} region indicates the presence of mass fractals with dimension of D = 1.2 (pH 4.84 supernatant) and 2.8 (pH 4.84), respectively.